Studies of Electron Cloud Growth and Mitigation in Dipole and Quadrupole Fields Using Retarding Field Analyzers

J.R. Calvey, M.G. Billing, J.V. Conway, G. Dugan, S. Greenwald, Y. Li, X. Liu, J.A. Livezey, J. Makita, R.E. Meller, M.A. Palmer, S. Santos, R.M. Schwartz, J. Sikora, C.R. Strohman, CLASSE, Cornell University, Ithaca, NY, USA
S. Calatroni, G. Rumolo, CERN, Geneva, Switzerland
K. Kanazawa, Y. Suetsugu, KEK, Ibaraki, Japan
M. Pivi, L. Wang, SLAC, Menlo Park, CA, USA
(Dated: November 1, 2012)

Over the course of the past three years, the Cornell Electron Storage Ring (CESR) has been reconfigured to serve as a test accelerator (CESRTA) for next generation machines, in particular for the ILC damping ring. A significant part of this program has been the installation of diagnostic devices to measure and quantify the electron cloud effect, a potential limiting factor in these machines. In particular, several Retarding Field Analyzers (RFAs) have been installed in CESR. These devices provide information on the local electron cloud density and energy distribution, and have been used to evaluate the efficacy of different cloud mitigation techniques. This paper will provide an overview of RFA results obtained in dipole and quadrupole field environments. Understanding these results provides a great deal of insight into the behavior of the electron cloud.

PACS numbers: 29.20.db, 52.35.Qz, 29.27.-a

I. INTRODUCTION

A summary of the CesrTA program, as well as detailed description of measurements and simulations in a field free environment, can be found in [1]. This paper will focus on results obtained in dipole and quadrupole field regions instrumented with RFAs.

II. INSTRUMENTATION

A more detailed description of the design and construction of the dipole and quadrupole RFAs can be found in [2]; here we present only a brief overview.

RFA data have been taken in the presence of a dipole field, both in a standard CESR dipole (Fig. 1), and in a specially designed chicane which was built at SLAC [3] (Fig. 2. The field in the chicane magnets is variable, but most of our measurements were done in a nominal dipole field of 810G. Of the four chicane chambers, one is bare Aluminum, two are TiN coated, and one is both grooved and TiN coated. The grooves are triangular with a depth of 5.6mm and an angle of 20°.

Another development at CesrTA has been the incorporation of an RFA into a quadrupole chamber (Fig. 3). This RFA wraps azimuthally around the chamber, from about 70 to 150 degrees (taking zero degrees to be the source point).

Table I provides a summary of dipole and quadrupole RFA styles deployed in CESR.

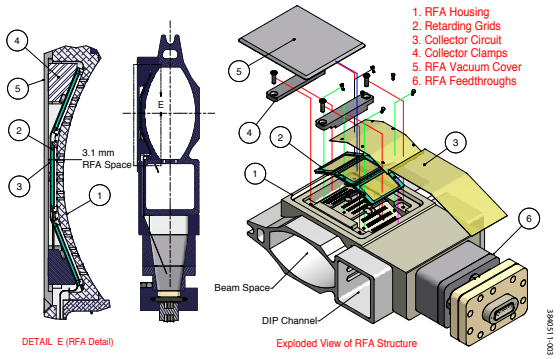

FIG. 1: RFA design detail for a CESR dipole chamber.

TABLE I: Dipole/Quadrupole RFA styles deployed in CESR

Type	Grids	Collectors	Grid Transparency
CESR dipole	1	9	40%
SLAC chicane	3	17	90%
Quadrupole	1	12	90%

III. DIPOLE MEASUREMENTS

Most of the data presented here is one of two types: "voltage scans," in which the retarding voltage is varied (typically from +100 to -250V) while beam conditions are held constant, or "current scans," in which the retarding grid is set to a positive voltage (typically 50V), and data is passively collected while the beam current is increased.

Fig. 4 shows a retarding voltage scan done with both the CESR dipole and Aluminum chicane RFAs. In both cases, one can see a strong multipacting peak in the central collector. These can be compared with the TiN coated chicane RFA (Fig. 5), in which the peak is greatly

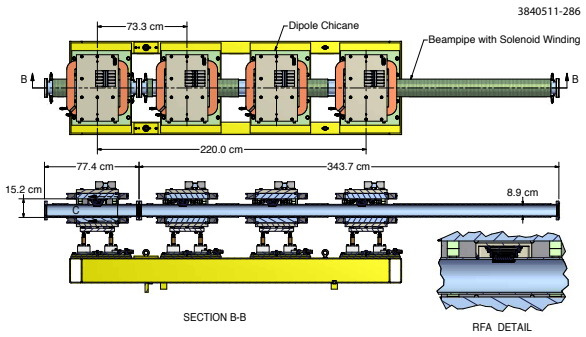

FIG. 2: PEP-II 4-dipole magnet chicane and RFA-equipped EC chambers.

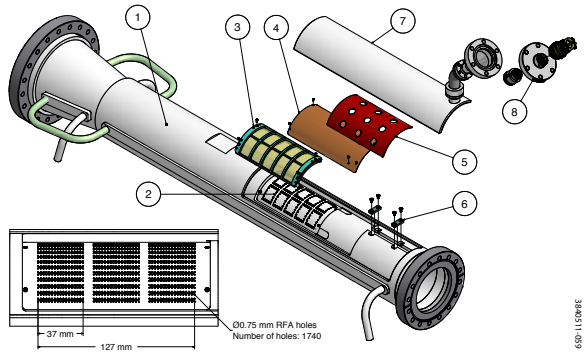

FIG. 3: Exploded view of the structure of the RFA within a CESR quadrupole beam pipe. The major components of the RFA beam pipe include: (1) Aluminum beam pipe with cooling channels; (2) RFA housing and wiring channels; (3) Retarding grids, consisting of high-transparency gold-coated meshes nested in PEEK frames; (4) RFA collector flexible circuit; (5) Stainless steel backing plate; (6) Wire clamps; (7) RFA vacuum cover with connection port; (8) 19-pin electric feedthrough for RFA connector

suppressed.

A. Mitigation Comparisons

Fig. 6 shows a current scan comparison between three of the chicane RFAs. We observe a large difference between uncoated and coated chambers. At high beam current, the TiN coated chamber shows a signal smaller by two orders of magnitude than the bare Al chamber, while the coated and grooved chamber performs better still.

A similar comparison, done with an electron beam, is shown in Fig. 7. Here we observe a threshold current, at which the aluminum chamber signal "turns on," and shows a dramatic increase with current. This threshold is not observed in any of the mitigated chambers.

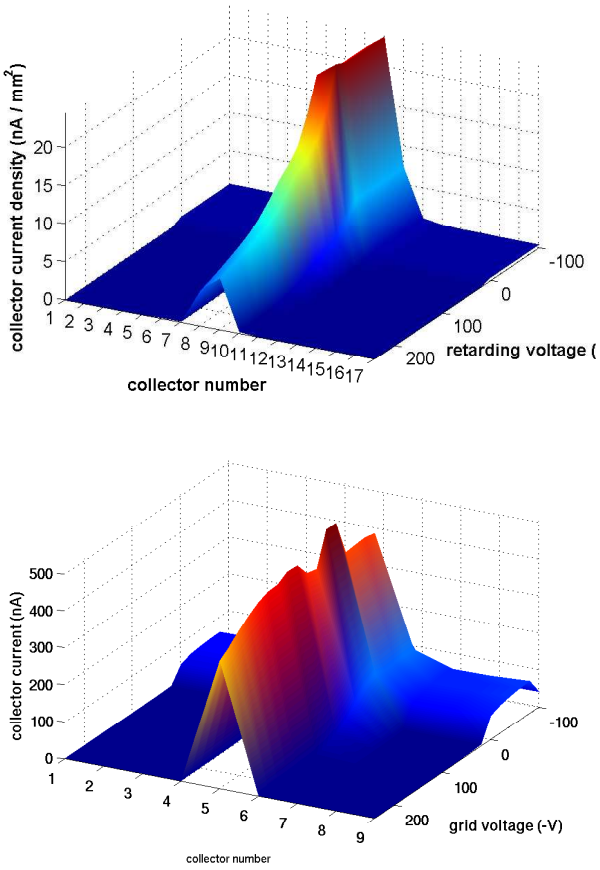

FIG. 4: Typical Al dipole RFA voltage scans: 1x45x1.25mA e+, 5.3GeV, 14ns. Top: SLAC chicane RFA (810 Gauss); Bottom: CESR dipole RFA (2011 Gauss)

B. Bifurcation of Central Peak

For high bunch currents, we have observed a bifurcation of the central multipacting peak into two peaks with a dip in the middle. This is demonstrated in Fig 8, which shows the signal in all 17 RFA collectors vs beam current. Bifurcation occurs when the average energy of electrons in the center of the beam pipe is past the peak of the SEY curve, so that the effective maximum yield is actually off center. The higher the bunch current, the further off center these peaks will be.

C. Cyclotron Resonances

By varying the strength of the chicane magnets, we can also study the behavior of the cloud at different dipole magnetic field values. Fig. 9 shows an example of RFA data taken as a function of magnetic field strength. The most prominent feature of the data is regularly occurring spikes or dips in all three plotted chambers. These correspond to "cyclotron resonances," which occur whenever the cyclotron period of cloud electrons is an integral mul-

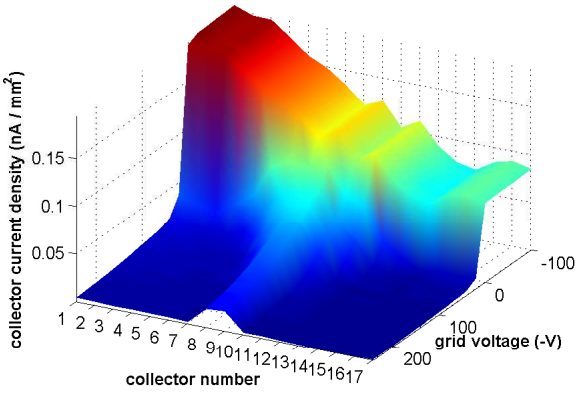

FIG. 5: Voltage scan in TiN coated chicane chamber: 1x45x1.25mA e+, 5.3GeV, 14ns.

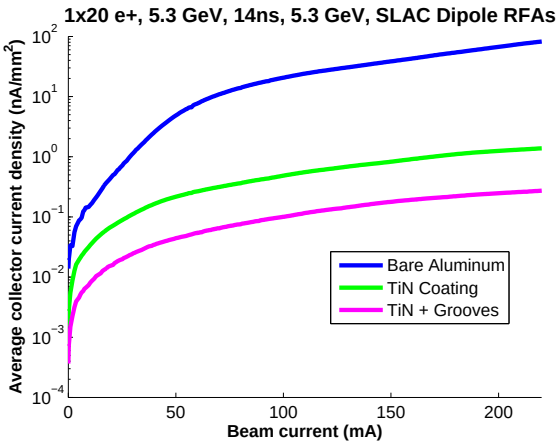

FIG. 6: Dipole RFA mitigation comparison, 1x20 e+, 5.3GeV, 14ns

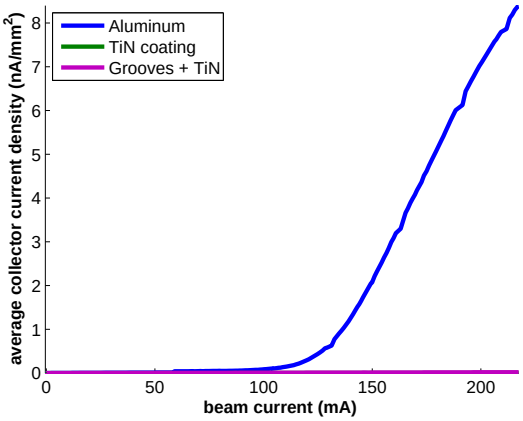

FIG. 7: Dipole RFA mitigation comparison, 1x20 e-, 5.3GeV, 14ns

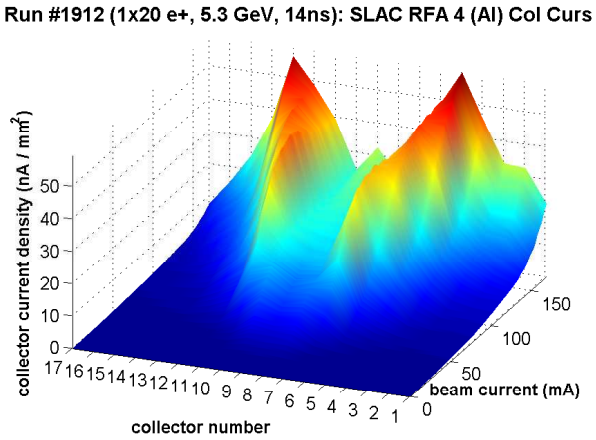

FIG. 8: Bifurcation of peak cloud density in a Al dipole: 1x20 e+, 5.3GeV, 14ns

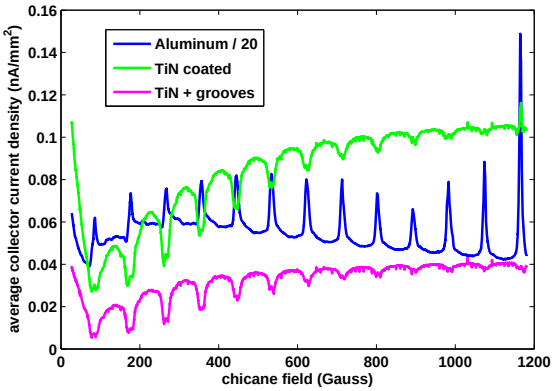

FIG. 9: RFA signal as a function of chicane magnetic field: 1x45x1mA e+, 5GeV, 4ns. Cyclotron resonances are observed every 89G. Note that the Aluminum chamber signal is divided by 20.

tiple of the bunch spacing [4]. For 4ns bunch spacing we expect them every 89 Gauss, which is what is seen in the data. Another interesting feature of this measurement is that these resonances appear as peaks in the RFA signal in the Aluminum chamber, but as dips in the coated chambers.

D. Bunch Spacing Studies

Because the properties of the electron cloud can change over the course of nanoseconds, it is interesting to investigate its behavior as a function of bunch spacing. At CesrTA we have taken RFA data with bunch spacings varying from 4ns to 112ns.

Fig. 10 shows the signal in the central collector of two dipole RFAs as a function of bunch spacing. The left plot is for the Aluminum SLAC chicane RFA; the right is for the CESR dipole RFA (see Fig. 4). The SLAC chamber

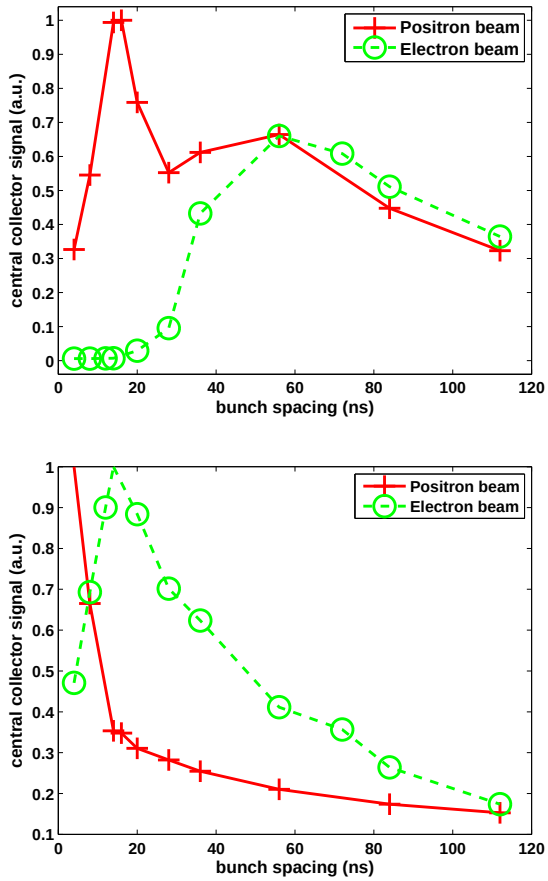

FIG. 10: Central collector signal in a dipole RFA as a function of bunch spacing, for a 20 bunch train with 3.5mA (5.6×10^{10} particles) per bunch, at 5.3 GeV. Top: SLAC chicane RFA, bottom: CESR dipole RFA

has a half-height of 4.4cm, while the CESR RFA has a half-height of 2.5cm.

For the SLAC RFA, we observe two distinct peaks in the positron data, at approximately 14ns and 60ns. The electron beam data shows almost no signal before 36ns, and is peaked around the same place as second the positron peak. The enhancement of the signal at 60ns could be due to a resonance between the bunch spacing and the cloud development (often called a "multipacting resonance"). This effect will be enhanced by the dipole field, which renders the motion of the electrons mostly one dimensional.

A very simple model for a multipacting resonance is that if the time for a typical secondary electron to travel to the center of the beam pipe is equal to the bunch spacing, this electron will be kicked strongly by the beam, and is likely to produce more secondary electrons. In reality, peak secondary production will occur when this electron is given an amount of energy corresponding to the peak of the SEY curve. However, for aluminum the SEY is greater than 1 well into the keV range, so an electron anywhere near the beam is a candidate to produce more secondaries. Thus we expect the "resonance" to be somewhat broad.

If we ignore the time for the kicked electron to travel to the beam pipe wall (which will be small if the kick is strong), the resonance condition is simply $t_b = a/v_{sec}$, where t_b is the bunch spacing, a is the chamber half-height (i.e. the distance from the wall to the beam), and v_{sec} is a characteristic secondary electron velocity. For a 1.5eV electron, this peak will occur at 61ns. The fact that there is a finite width to the secondary energy distribution will further smear out the peak.

The lower energy peak in the positron data could be a higher order multipacting resonance, where it takes two bunches to set up the resonance condition. Here we consider the case where the first bunch gives some additional energy to the electron, so that it makes it to the center of the chamber in time for the second bunch. If we again neglect the time for the kicked electron to reach the beam pipe wall, the resonance condition becomes:

$$t_{b,2} = \frac{a-r_1}{v_{sec}} = \frac{r_1}{v_2} \quad (1)$$

$$v_2 = v_{sec} + \frac{2cN_b r_e}{r_1} \quad (2)$$

Here r_1 is the distance from the electron to the beam during the first bunch passage, v_2 is the velocity of the electron after it is kicked by the first bunch, N_b is the bunch population and r_e is the classical electron radius. Solving for $t_{b,2}$ gives us Eq. 3, where we have defined $k \equiv 2cN_b r_e$.

$$t_{b,2} = \frac{k + 3av_{sec} - \sqrt{k^2 + 6kav_{sec} + a^2 v_{sec}^2}}{4v_{sec}^2} \quad (3)$$

For a 1.5eV secondary electron, $t_{b,2}$ is 11ns, somewhat less than the 14ns that is observed. A more sophisticated model (which would include, among other things, the time for the kicked electron to reach the wall) may yield a more accurate result. Note that this resonance condition applies only to positron beams, so only one peak is predicted for the electron data (which is what we find). Overall, a multipacting scenario with a 1.5eV peak secondary energy is approximately consistent with the SLAC chicane data, for both the positron and electron beam data.

The predictions for our CESR dipole (Fig. 10, right) would then be $t_b = 34$ns and $t_{b,2} = 4$ns. The former is higher than what is observed, though the latter is consistent with the data. A better fit would be for an 8eV electron, then $t_b = 15$ns and $t_{b,2} = 3$ns. It is also possible that a more sophisticated model would fit the CESR dipole data better.

IV. QUADRUPOLE DATA

A typical quadrupole RFA measurement is shown in Fig. 11. We find that the collector that is lined up with

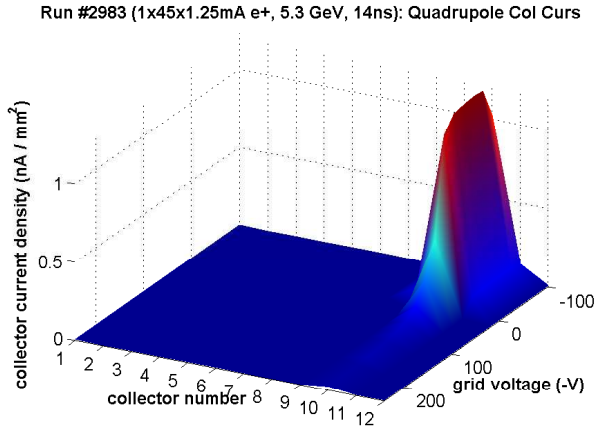

FIG. 11: Quadrupole RFA voltage scan: 1x45x1.25mA e+, 5.3GeV, 14ns

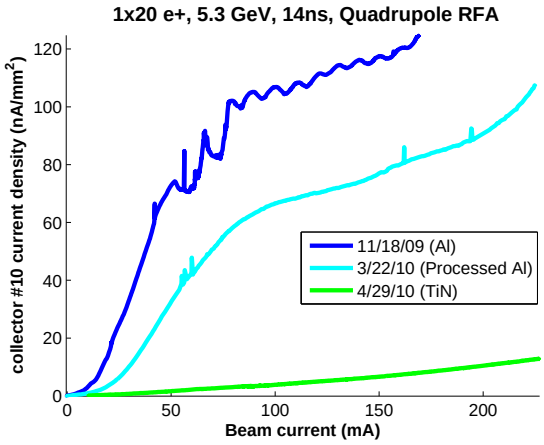

FIG. 12: Quadrupole mitigation comparison, 1x20 e+, 5.3GeV, 14ns

the quad pole tip (no. 10) sees a large amount of current, while the rest of the collectors see relatively little. This suggests that the majority of the cloud in the quad is streaming between two pole tips.

A. Mitigation Comparison

Fig. 12 shows a comparison of a bare Aluminum (both processed and unprocessed) quadrupole chamber with the TiN coated chamber that has replaced it. In this comparison only collector 10 is being plotted. The signal in the TiN chamber was found to be reduced by well over an order of magnitude.

B. Bunch Spacing Study

One potential side effect of the cloud mirroring between the quad pole tips is that it may become trapped

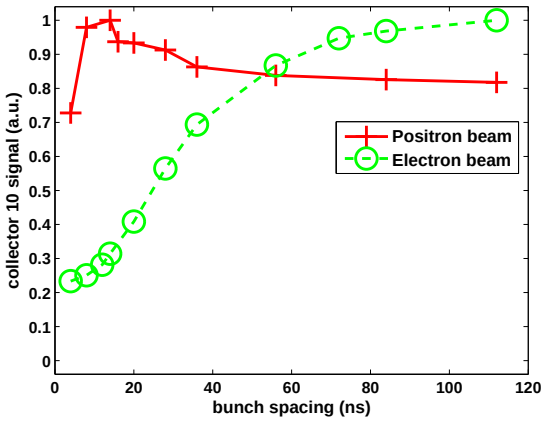

FIG. 13: Signal in a quadrupole RFA as a function of bunch spacing, for the same beam conditions as in Fig. 10. The collector which is in line with the quad pole tip is plotted.

for a long time. As seen in Fig. 13, for a positron beam we do not observe a strong dependence on bunch spacing, though there does seem to be a modest enhancement around 14ns. The data for an electron beam is even more surprising, actually showing a monotonic increase with bunch spacing. Both of these measurements are consistent with a timescale for cloud development in the quad that is much longer than 100ns.

V. DIPOLE SIMULATIONS

A model for both types of dipole RFA has been incorporated into POSINST [5], and predicted RFA signals are produced automatically by the simulation [1].

Modeling an RFA in a dipole magnetic field presents a unique set of challenges. Fig. 15 shows the efficiency (probability of making it through the beam pipe hole) as a function of incident angle in this RFA, calculated using a specialized particle tracking code [1]. Note that low energy particles have a very high efficiency, due to their small cyclotron radius.

Fig. 15 compares a simulation done for the CESR dipole RFA, under standard beam conditions. The agreement with the data is very good for a retarding voltage $\geq 20\ V$, but the simulation overestimates the low energy signal by a factor of 3. This is because in a strong dipole field, electrons are mostly pinned to the field lines, and do not move very far transversely. So in a real measurement, the RFA will deplete the cloud in precisely the region it is sampling, i.e. under the beam pipe holes. Not taking this into account will result in an overestimate of the RFA signal, especially at low energy (where the electrons are strongly pinned to the field lines).

Accurately modeling the locations of the holes means that only a fraction of the macroparticles colliding with the top of the vacuum chamber will produce an RFA signal. This increases the statistical error in the simulation

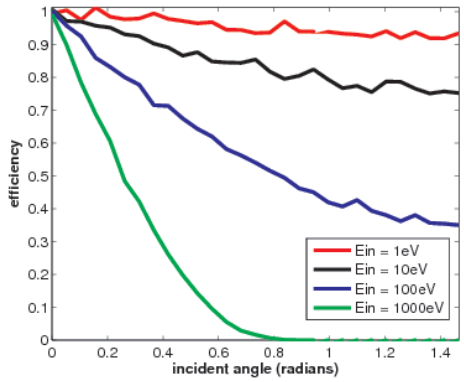

FIG. 14: Simulated RFA efficiency vs incident angle for a SLAC chicane dipole RFA, with a .081 T magnetic field.

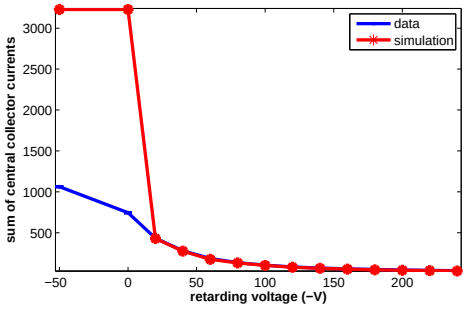

FIG. 15: Measured and simulated RFA signal, in the CESR dipole RFA: 1x45x1.25 mA e+, 14 ns, 2.1 GeV

results, and slows down the analysis. Nonetheless, this more accurate model is currently being implemented.

VI. QUADRUPOLE SIMULATIONS

Some preliminary simulations have been done for the quadrupole RFA installed in CESR. The simulations reproduce the behavior described above, where the majority of the signal is concentrated in one collector. Interestingly, they also give some indirect evidence that the cloud can become trapped in the quadrupole for long periods of time.

Fig 16 shows the signal in collector no. 10 for a voltage scan done with a 45 bunch train of positrons at 1mA/bunch. Also plotted are simulations done in ECLOUD [6] of these conditions. If one does a simulation for only one beam revolution period (2.56μs), the simulated signal is too low at all energies by over an order of magnitude. However, if one continues the simulation for multiple turns, one finds that the data and simulation start to get closer. By 19 turns, they are in very good agreement at high energy, and within a factor of 2 at low energy. This implies that the cloud is building up over several turns, and that the RFA is sensitive to this slow buildup.

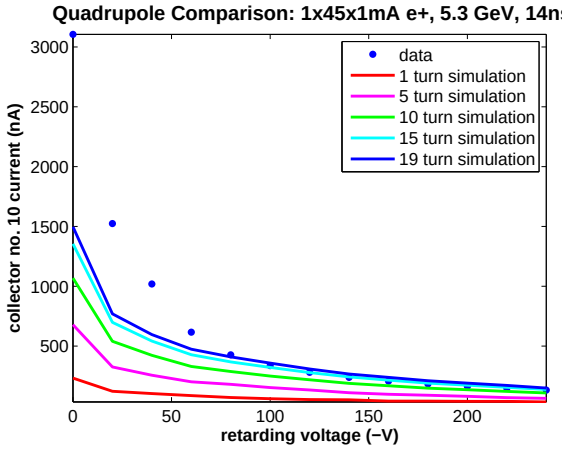

FIG. 16: Quadrupole RFA simulation showing long term cloud buildup: 45 bunches, 1mA/bunch, e+, 5.3 GeV, 14ns

VII. CONCLUSIONS

Retarding field analyzers have been used to study the electron cloud in dipole and quadrupole field environments. Interesting phenomena, including peak bifurcation, cyclotron resonances, and multipacting resonances have been observed in a dipole. We also have some evidence that long term cloud trapping can occur in a quad. TiN coating was shown to be effective for mitigating the cloud in both dipoles and quadrupoles, while TiN coated grooves were even more effective in a dipole. The presence of a magnetic field makes simulations of the RFA signals more complicated; nonetheless basic simulations for dipole and quads have been performed.

[1] J. C. et. al., Phys. Rev. ST Accel. Beams **A598**, 372 (2012).

[2] M. Palmer, M. Billing, G. Dugan, D. Rubin, and M. Furman, Tech. Rep., LEPP, Cornell University, Ithaca, NY (2012), URL `https://wiki.lepp.cornell.edu/ilc/bin/view/Public/CesrTA/CesrTAPhaseIReport`.

[3] M. T. F. Pivi, J. S. T. Ng, F. Cooper, D. Kharakh, F. King, R. E. Kirby, B. Kuekan, C. M. Spencer, T. O. Raubenheimer, and L. F. Wang, Nucl. Instrum. Methods Phys. Res. **A621**, 33 (2010).

[4] C. M. Celata, M. A. Furman, J.-L. Vay, D. P. Grote, J. S. T. Ng, M. T. F. Pivi, and L. F. Wang, in *Proceedings of the 2009 Particle Accelerator Conference, Vancouver, BC* (2009), pp. 1807–1811, URL `http://accelconf.web.`

cern.ch/AccelConf/PAC2009/papers/we1pbi03.pdf.

[5] M. A. Furman and M. T. F. Pivi, Phys. Rev. ST Accel. Beams **5**, 124404 (2002).

[6] F. Zimmermann, G. Rumolo, and K. Ohmi, in *ICFA Beam Dynamics Newsletter*, edited by K. Ohmi and M. Furman (International Committee on Future Accelerators, 2004), No. 33, pp. 14–24, URL http://wwwslap.cern.ch/collective/electron-cloud/zimmermann/ICFA/ecloudbuildup.pdf.